

# GEOMETRIC KERNEL INTERPOLATION AND REGRESSION

PATRICK GUIDOTTI

**ABSTRACT.** Exploiting the variational interpretation of kernel interpolation we exhibit a direct connection between interpolation and regression, where interpolation appears as a limiting case of regression. By applying this framework to point clouds or samples of smooth manifolds (hypersurfaces, in particular), we show how fundamental geometric quantities such as tangent plane and principal curvatures can be computed numerically using a kernel based (approximate) level set function (often a defining function) for smooth hypersurfaces. In the case of point clouds, the approach generates an interpolated hypersurface, which is an approximation of the underlying manifold when the cloud is a sample of it. It is shown how the geometric quantities obtained can be used in the numerical approximation/computation of geometric operators like the surface gradient or the Laplace-Beltrami operator in the spirit of kernel based meshfree methods. Kernel based interpolation can be extremely ill-posed, especially when using smooth kernels, and the regression approximation offers a natural regularization that proves also quite useful when dealing with geometric or functional data that are affected by errors or noise.

## 1. INTRODUCTION

Kernel Methods play an important role in interpolation theory as they nicely bridge the gap between infinite dimensional function spaces and finite dimensional approximations thereof. We shall make this statement more precise below when we highlight the optimization aspect of kernel interpolation. Kernel methods are meshfree methods that come with a solid theoretical foundation [10, 34]. They can be used for interpolation as well as for a variety of other purposes that range from the numerical resolution of differential equations and (initial) boundary value problems to classification and statistical learning [28]. A particularly relevant connection to Gaussian Process Regression will be briefly discussed as it provides an alternative justification for the regularized kernel-based “quasi”-interpolation that proves useful in the context of noisy data.

The main contribution of this paper consist of the realization, new to the best of our knowledge, and subsequent exploitation, of the fact that kernel methods (and the related regression methods) can be used directly to construct viable “defining” (level set) functions of hypersurfaces (or more general submanifolds), which then give direct access to global (localizable) interpolation of their geometric properties (normals and curvatures) starting with a (not necessarily uniform) sample of their points (the point cloud). With these in hand, it also becomes possible to stably compute geometric operators of functions simply given through their values on the unstructured (sampling) point cloud in the spirit of meshfree methods. The point cloud (sample) is viewed as a discrete embedding and the proposed use of kernel methods combined with formulae in terms of ambient space coordinates yields numerical discretizations in extrinsic coordinates. In other words, geometric quantities and operators can be computed directly from the point cloud and applied to functions defined on it. The approximate computation of curvatures and differential operators on manifolds is immediately relevant within applied mathematics and numerical analysis as they can directly be employed in order to numerically solve a variety of natural PDEs on manifolds. It does, however, also play an important role in computer graphics and vision ([21, 31, 23]). The use of geometric operators can also be used in the case of noisy or corrupted samples. Following ideas first pioneered in a full space context, denoising of (surface) meshes can, for instance, be performed by using normal motion by mean curvature (see [8]). The

---

*Key words and phrases.* Kernel based interpolation and regression, point cloud interpolation and analysis, functions and operators on point clouds.

approach to corrupted or noisy clouds taken here does not require explicitly evolving the noisy sample since denoising is implicit and automatic in the sense that the regularization yielding approximate interpolation or regression results in smoother level sets of the approximate interpolant. Numerical access to geometric information is also of interest in applications beyond denoising. Examples of such applications are mesh simplification ([14, 18]), surface modeling [24], and fairing of meshes [6], where a formulation as a Laplace-Beltrami diffusion of the coordinates is used. Other applications include surface reconstruction [2], shape recognition or registration [15], cortical morphology and organ shape analysis (see e.g. [11, 7, 29]), and many more. It is worth mentioning that, contrary to what is typically done in the literature [4, 34, 10, 27], we work with the point cloud itself without augmenting it with two layers of additional points placed at a fixed distance from the surface in normal and negative normal direction (which requires additional knowledge about the normal vectors and introduces additional parameters that influence the accuracy of the method). Finally the approach is meshfree and, as such, does not require a sophisticated structured representation of the surfaces of interest and, in fact, in a smooth context, works also with non-necessarily dense or regular discretizations/samples as will be shown in the final section.

The analysis proposed in this paper offers some new insights but also integrates many previous observations that have appeared in the kernel interpolation and radial basis function literature (including applications to PDEs), in applications to visualization for the reconstruction, representation, and processing of curves and surfaces, and in the statistical literature.

It was already observed in [13] that positive definite full space kernels  $K : \mathbb{R}^d \times \mathbb{R}^d \rightarrow \mathbb{R}$ , can be used to perform interpolation of functions defined on embedded manifolds  $\mathcal{M} \subset \mathbb{R}^d$ , not necessarily of codimension one. In [27] it is shown how radial basis functions can be successfully employed in order to compute numerical solution to PDEs on surfaces. The use of kernel interpolation for scattered data is also discussed in [34], where one also finds an exhaustive treatment of positive kernels, kernel interpolation theory, approximation results, and much more. Finally, the spline based regression introduced in [32] also exploits the structure and framework provided by general kernel methods even if in a specific incarnation and was used in [4] for dealing with noisy surface data in a similar way as it is done here in a more general context. We shall give additional detail in the following sections. Finally there is also a natural connection to manifold learning but we refer to [17] for a more thorough discussion of this aspect.

## 2. KERNEL INTERPOLATION

While we refer the reader to the literature [33, 10] for a comprehensive account of kernel methods, we provide a brief introduction here with the goal of revealing the insight that leads to the geometric use announced in the introduction.

**Definition 2.1.** *An at least continuous kernel  $K : \mathbb{R}^d \rightarrow \mathbb{R}$  is called positive definite if and only if the matrix*

$$K(\mathbb{X}, \mathbb{X}) = [K(x_j - x_k)]_{1 \leq j, k \leq |\mathbb{X}|} \in \mathbb{R}^{|\mathbb{X}| \times |\mathbb{X}|}$$

*is symmetric positive definite for every choice of a set  $\mathbb{X} = \{x^1, \dots, x^{|\mathbb{X}|}\}$  containing  $|\mathbb{X}| < \infty$  distinct points.*

This allows one to use  $\{K(\cdot - x_k) \mid k = 1, \dots, |\mathbb{X}|\}$  as “basis functions” in the interpolation problem consisting of finding a function  $f : \mathbb{R}^d \rightarrow \mathbb{R}$  with  $f(x^j) = y^j \in \mathbb{R}$  for  $j = 1, \dots, |\mathbb{X}|$ , or  $f(\mathbb{X}) = \mathbb{Y}$  for short. Indeed the corresponding system takes the form

$$\left( \sum_{k=1}^{|\mathbb{X}|} K(\cdot - x^k) \lambda_k \right) \big|_{\mathbb{X}} = K(\mathbb{X}, \mathbb{X}) \Lambda = \mathbb{Y}$$

and is solvable whenever  $K$  is positive definite. In this way, one obtains an everywhere defined interpolant

$$u_{\mathbb{X}, \mathbb{Y}} = K(\cdot, \mathbb{X})K(\mathbb{X}, \mathbb{X})^{-1}\mathbb{Y}. \quad (2.1)$$

The usefulness and power of the method stems from the fact that it is possible to associate to  $K$  an infinite dimensional Hilbert space of functions  $\mathcal{H}_K$ , the so-called reproducing kernel Hilbert space, often known as the native space, with the remarkable property that

$$u_{\mathbb{X}, \mathbb{Y}} = \operatorname{argmin}_{u(\mathbb{X})=\mathbb{Y}} E_0(u), \quad E_0(u) = \frac{1}{2}\|u\|_{\mathcal{H}_K}^2. \quad (2.2)$$

The Hilbert space  $\mathcal{H}_K$  is the completion of the finite linear combinations  $K(\cdot, \mathbb{X})\alpha = \sum_{k=1}^{|\mathbb{X}|} \alpha_k K(\cdot - x^k)$  with norm defined by

$$(K(\cdot, \mathbb{X}_1)\alpha^1 | K(\cdot, \mathbb{X}_2)\alpha^2) = (\tilde{\alpha}^1)^\top K(\mathbb{X}, \mathbb{X})\tilde{\alpha}^2,$$

where  $\mathbb{X} = \mathbb{X}_1 \cup \mathbb{X}_2$  and  $\tilde{\alpha}_i \in \mathbb{R}^{|\mathbb{X}|}$  is the trivial extension of the vector  $\alpha_i \in \mathbb{R}^{|\mathbb{X}_i|}$  obtained by setting to zero the missing components corresponding to  $\mathbb{X}_i \setminus \mathbb{X}_j$  ( $j \neq i$ ) for  $i = 1, 2$ .

**Remarks 2.2.** (a) The fact that the minimizer has the form  $K(\cdot, \mathbb{X})\Lambda$  for some  $\Lambda \in \mathbb{R}^{|\mathbb{X}|}$  goes by the name Representer Theorem in the more applied literature.

(b) The name Reproducing Kernel Hilbert Space (RKHS) is justified by the central property that

$$\int K(x - y)u(y) dy = u(x), \quad x \in \mathbb{R}^d,$$

for every  $u \in \mathcal{H}_K$ . If  $u$  is replaced by a translate of the kernel, the integration yields back the kernel itself. This formula also shows that  $\delta_x \in \mathcal{H}_K^*$ .

In order to introduce the proposed extension, we now turn things on their head and start with the optimization problem (2.2) for which it is natural to consider the closely related problem

$$\operatorname{argmin}_{u \in \mathcal{H}_K} \frac{1}{2} \left\{ \|u\|_{\mathcal{H}_K}^2 + \frac{1}{\alpha} |u(\mathbb{X}) - \mathbb{Y}|^2 \right\} = \operatorname{argmin}_{u \in \mathcal{H}_K} E_\alpha(u) \quad (2.3)$$

for  $\alpha > 0$ . One can think of Problem (2.2) as the pure interpolation problem and of (2.3) as the approximate interpolation or regression problem. For these problems we have the following basic results.

**Proposition 2.3.** The optimization problems (2.3),  $\alpha > 0$ , and (2.2) possess a unique minimizer  $u_{\mathbb{X}, \mathbb{Y}}^\alpha \in \mathcal{H}_K$ . For  $\alpha > 0$ , the minimizer  $u_{\mathbb{X}, \mathbb{Y}}^\alpha$  is a weak solution of the equation

$$\mathcal{A}_K u = \frac{1}{\alpha} [\mathbb{Y} - u(\mathbb{X})]^\top \delta_{\mathbb{X}} = \frac{1}{\alpha} \sum_{k=1}^{|\mathbb{X}|} [y^k - u(x^k)] \delta_{x^k}, \quad (2.4)$$

i.e. a solution of the equation in  $\mathcal{H}_K^*$ . If  $\alpha = 0$ , then it holds that

$$\mathcal{A}_K u_{\mathbb{X}, \mathbb{Y}}^0 = \Lambda^\top \delta_{\mathbb{X}} = \sum_{k=1}^{|\mathbb{X}|} \lambda_k \delta_{x^k}$$

for some Lagrange multiplier  $\Lambda \in \mathbb{R}^{|\mathbb{X}|}$ . The operator  $\mathcal{A}_K$  is defined by the validity of the identity  $(u|\varphi)_{\mathcal{H}_K} = \langle \mathcal{A}_K u, \varphi \rangle_{\mathcal{H}_K^*, \mathcal{H}_K}$  for  $u, \varphi \in \mathcal{H}_K$ , i.e. it coincides with the Riesz isomorphism. The coefficient vector  $\Lambda$  is obtained from the augmented Lagrangian  $E_0(u) - \Lambda^\top (u(\mathbb{X}) - \mathbb{Y})$ .

*Proof.* As the functionals are convex, existence and uniqueness readily follow (and is already known for  $\alpha = 0$  as discussed earlier). Taking variations in direction of functions  $\varphi \in \mathcal{H}_K$  with  $\varphi(\mathbb{X}) = 0$  shows that  $\mathcal{A}_K u_{\mathbb{X}, \mathbb{Y}}^0 \in N_{\mathbb{X}}^\perp$ , where  $N_{\mathbb{X}} = \{\varphi \in \mathcal{H}_K \mid \varphi(\mathbb{X}) = 0\}$ , which yields the representation formula that can also be obtained by taking variations with respect to the  $u$  variable in the augmented Lagrangian to see that

$$0 = (u|\varphi)_{\mathcal{H}_K} - \Lambda^\top \varphi(\mathbb{X}) = \langle \mathcal{A}_K u - \Lambda^\top \delta_{\mathbb{X}}, \varphi \rangle, \quad \varphi \in \mathcal{H}_K.$$

Taking variations of  $E_\alpha$ ,  $\alpha > 0$ , yields that

$$0 = (u|\varphi)_{\mathcal{H}_K} + \frac{1}{\alpha} (u(\mathbb{X}) - \mathbb{Y}) \cdot \varphi(\mathbb{X}) = \langle \mathcal{A}_K u + \frac{1}{\alpha} (u(\mathbb{X}) - \mathbb{Y})^\top \delta_{\mathbb{X}}, \varphi \rangle, \varphi \in \mathcal{H}_K,$$

which is the desired weak equation.  $\square$

**Remark 2.4.** *The identity*

$$(\mathcal{A}_K^{-1} \delta_x)(\tilde{x}) = (\mathcal{A}_K^{-1} \delta_x | k(\cdot, \tilde{x}))_{\mathcal{H}_K} = \langle \mathcal{A}_K \mathcal{A}_K^{-1} \delta_x, k(\cdot, \tilde{x}) \rangle = k(x, \tilde{x})$$

identifies the kernel as a fundamental solution of the operator  $\mathcal{A}_K$  leading to the Ansatz

$$u = \Lambda^\top \mathcal{A}_K^{-1} \delta_{\mathbb{X}} = K(\cdot, \mathbb{X}) \Lambda,$$

and to the equation  $\mathbb{Y} = u(\mathbb{X}) = K(\mathbb{X}, \mathbb{X}) \Lambda$ .

**Remark 2.5.** *The Laplace kernel  $L(x) = e^{-|x|}$ ,  $x \in \mathbb{R}^d$ , is a fundamental solution of the operator  $c_d(1 - 4\pi^2 \Delta)^{\frac{d+1}{2}}$  for  $c_d = \frac{\pi^{\frac{d+1}{2}}}{\Gamma(d+1)}$  and is therefore a positive kernel (thanks to the characterization of positivity via its Fourier transform, i.e. thanks to Bochner's Theorem, see e.g. [34]) with native space given by  $H^{\frac{d+1}{2}}(\mathbb{R}^d)$ . It is a kernel with low regularity and is a special case of a kernel family known as Matérn kernels [22] that includes kernels of higher and higher regularity.*

*Proof.* This can be derived e.g. from the results about Bessel Potentials found in [1].  $\square$

**Corollary 2.6.** *The minimizer  $u_{\mathbb{X}, \mathbb{Y}}$  of (2.2) has the form*

$$u_{\mathbb{X}, \mathbb{Y}} = K(\cdot, \mathbb{X}) K(\mathbb{X}, \mathbb{X})^{-1} \mathbb{Y}.$$

*The Ansatz  $u_{\mathbb{X}, \mathbb{Y}}^\alpha = K(\cdot, \mathbb{X}) \Lambda$  can be also used for the minimizer of (2.3) and gives*

$$\Lambda = (\alpha + K(\mathbb{X}, \mathbb{X})^{-1} \mathbb{Y}).$$

*Proof.* Plugging the Ansatz into the equation satisfied by  $u_{\mathbb{X}, \mathbb{Y}}^\alpha$  gives

$$\Lambda^\top \delta_{\mathbb{X}} + \frac{1}{\alpha} [K(\cdot, \mathbb{X}) \Lambda]^\top \delta_{\mathbb{X}} = \Lambda^\top \delta_{\mathbb{X}} + \frac{1}{\alpha} [K(\mathbb{X}, \mathbb{X}) \Lambda]^\top \delta_{\mathbb{X}} = \frac{1}{\alpha} \mathbb{Y}^\top \delta_{\mathbb{X}},$$

which, by linear independence of evaluations at distinct points implies that

$$\alpha \Lambda + K(\mathbb{X}, \mathbb{X}) \Lambda = \mathbb{Y},$$

as claimed.  $\square$

Notice that the above results show how, in this particular setup, it is possible to reduce the identification of a solution to the infinite dimensional problem to the solution of a finite matrix problem.

**Remark 2.7.** *It was observed in [17] that the optimization problems (2.2) and (2.3) in the special case when  $K = L$  have infinite dimensional counterparts that allow for a similar “reduction in size”. Indeed, letting  $\mathcal{M} \subset \mathbb{R}^d$  be an orientable compact smooth submanifold, then one can consider*

$$\operatorname{argmin}_{u \in \mathcal{H}_K} \frac{1}{2} \left\{ \|u\|_{\mathcal{H}_K}^2 + \frac{1}{\alpha} \int_{\mathcal{M}} (u - f)^2 d\sigma_{\mathcal{M}} \right\}$$

for  $\alpha \geq 0$  with the understanding that, when  $\alpha = 0$  the functional loses its second term that is replaced by the constraint  $u|_{\mathcal{M}} = f$ . Arguments parallel to the ones used above lead to the reduced equations

$$\alpha u(x) + \int_{\mathcal{M}} L(x - y) u(y) d\sigma_{\mathcal{M}}(y) = f(x), \quad x \in \mathcal{M},$$

on the manifold  $\mathcal{M}$  (which replaces the cloud  $\mathbb{X}$ ) for  $f : \mathcal{M} \rightarrow \mathbb{R}$  (in place of  $\mathbb{Y}$ ). This analogy shows, on the one hand, that kernel interpolation amounts to solving a Fredholm integral equation of the first kind (i.e. a rather ill-posed problem), while approximate interpolation corresponds to solving a better conditioned second kind Fredholm integral equation. Regression, in this light, appears to be a natural regularization of exact interpolation.

There is a natural connection between (2.3) and (2.2).

**Proposition 2.8.** *Let  $u_{\mathbb{X}, \mathbb{Y}}^\alpha$  be the minimizer of (2.3) for  $\alpha > 0$  and of (2.2) for  $\alpha = 0$ . Denote the corresponding minima by  $e_\alpha$ ,  $\alpha \geq 0$ , and let  $0 < \alpha_0 < \alpha_1$ . Then it holds that*

- (i)  $u_{\mathbb{X}, \mathbb{Y}}^\alpha \rightarrow u_{\mathbb{X}, \mathbb{Y}}^0$  as  $\alpha \searrow 0$  in  $\mathcal{H}_K$ .
- (ii)  $0 \leq e_{\alpha_1} \leq e_{\alpha_0} \leq \frac{1}{2} \|u_{\mathbb{X}, \mathbb{Y}}^0\|_{\mathcal{H}_K}^2$  and  $|u_{\mathbb{X}, \mathbb{Y}}^{\alpha_0} - \mathbb{Y}|^2 \leq |u_{\mathbb{X}, \mathbb{Y}}^{\alpha_1} - \mathbb{Y}|^2$ .
- (iii)  $\|u_{\mathbb{X}, \mathbb{Y}}^{\alpha_1}\|_{\mathcal{H}_K} \leq \|u_{\mathbb{X}, \mathbb{Y}}^{\alpha_0}\|_{\mathcal{H}_K} \leq \|u_{\mathbb{X}, \mathbb{Y}}^0\|_{\mathcal{H}_K}$
- (iv)  $|u_{\mathbb{X}, \mathbb{Y}}^{\alpha_1} - \mathbb{Y}|^2 \leq \alpha [\|u_{\mathbb{X}, \mathbb{Y}}^0\|_{\mathcal{H}_K}^2 - \|u_{\mathbb{X}, \mathbb{Y}}^{\alpha_0}\|_{\mathcal{H}_K}^2]$ .

*Proof.* Notice that  $e_\alpha \leq e_0$  for  $\alpha > 0$  since  $u_{\mathbb{X}, \mathbb{Y}}^0 \in \mathcal{H}_K$  and  $E_\alpha(u_{\mathbb{X}, \mathbb{Y}}^0) = e_0$  where  $E_\alpha$  denotes the objective functional of (2.3). This entails that  $\|u_{\mathbb{X}, \mathbb{Y}}^\alpha\|_{\mathcal{H}_K} \leq C < \infty$  independently of  $\alpha > 0$ . In particular, we have that

$$0 \leq \frac{1}{2\alpha} |u_{\mathbb{X}, \mathbb{Y}}^\alpha(\mathbb{X}) - \mathbb{Y}|^2 \leq e_\alpha - \frac{1}{2} \|u_{\mathbb{X}, \mathbb{Y}}^\alpha\|_{\mathcal{H}_K}^2 \leq e_0 - \frac{1}{2} \|u_{\mathbb{X}, \mathbb{Y}}^0\|_{\mathcal{H}_K}^2 = \frac{1}{2} [\|u_{\mathbb{X}, \mathbb{Y}}^0\|_{\mathcal{H}_K}^2 - \|u_{\mathbb{X}, \mathbb{Y}}^\alpha\|_{\mathcal{H}_K}^2]$$

Given any null sequence  $(\alpha_k)_{k \in \mathbb{N}}$ , weak compactness yields a weakly convergent subsequence with limit  $u_{\mathbb{X}, \mathbb{Y}}^\infty \in \mathcal{H}_K$ , which, by weak lower semicontinuity of the norm, must satisfy  $\|u_{\mathbb{X}, \mathbb{Y}}^\infty\|_{\mathcal{H}_K}^2 \leq e_0$  and is therefore the unique minimizer  $u_{\mathbb{X}, \mathbb{Y}}^0$ . Define now  $d_{\mathbb{X}, \mathbb{Y}}^2(u) = |u(\mathbb{X}) - \mathbb{Y}|^2$  and notice that

$$\begin{aligned} e_{\alpha_0} &= \frac{1}{2\alpha_0} d_{\mathbb{X}, \mathbb{Y}}^2(u_{\mathbb{X}, \mathbb{Y}}^{\alpha_0}) + \|u_{\mathbb{X}, \mathbb{Y}}^{\alpha_0}\|_{\mathcal{H}_K}^2 \leq [\frac{1}{2\alpha_0} - \frac{1}{2\alpha_1}] d_{\mathbb{X}, \mathbb{Y}}^2(u_{\mathbb{X}, \mathbb{Y}}^{\alpha_1}) + \|u_{\mathbb{X}, \mathbb{Y}}^{\alpha_1}\|_{\mathcal{H}_K}^2 + \frac{1}{2\alpha_1} d_{\mathbb{X}, \mathbb{Y}}^2(u_{\mathbb{X}, \mathbb{Y}}^{\alpha_1}) \\ &\leq [\frac{1}{2\alpha_0} - \frac{1}{2\alpha_1}] d_{\mathbb{X}, \mathbb{Y}}^2(u_{\mathcal{M}}^{\alpha_1}) + \|u_{\mathbb{X}, \mathbb{Y}}^{\alpha_0}\|_{\mathcal{H}_K}^2 + \frac{1}{2\alpha_1} d_{\mathbb{X}, \mathbb{Y}}^2(u_{\mathbb{X}, \mathbb{Y}}^{\alpha_0}) \end{aligned}$$

yields that  $d_{\mathbb{X}, \mathbb{Y}}^2(u_{\mathbb{X}, \mathbb{Y}}^{\alpha_0}) \leq d_{\mathbb{X}, \mathbb{Y}}^2(u_{\mathbb{X}, \mathbb{Y}}^{\alpha_1})$ . Since

$$e_{\alpha_1} = \frac{1}{2\alpha_1} d_{\mathbb{X}, \mathbb{Y}}^2(u_{\mathbb{X}, \mathbb{Y}}^{\alpha_1}) + \|u_{\mathbb{X}, \mathbb{Y}}^{\alpha_1}\|_{\mathcal{H}_K}^2 \leq \frac{1}{2\alpha_1} d_{\mathbb{X}, \mathbb{Y}}^2(u) + \|u\|_{\mathcal{H}_K}^2 \leq \frac{1}{2\alpha_0} d_{\mathbb{X}, \mathbb{Y}}^2(u) + \|u\|_{\mathcal{H}_K}^2,$$

taking the infimum over  $u \in \mathcal{H}_K$  gives  $e_{\alpha_1} \leq e_{\alpha_0}$  as claimed. Next we have that

$$\|u_{\mathbb{X}, \mathbb{Y}}^{\alpha_1}\|_{\mathcal{H}_K}^2 \leq \|u_{\mathbb{X}, \mathbb{Y}}^{\alpha_0}\|_{\mathcal{H}_K}^2 - \frac{1}{2\alpha_1} [d_{\mathbb{X}, \mathbb{Y}}^2(u_{\mathbb{X}, \mathbb{Y}}^{\alpha_1}) - d_{\mathbb{X}, \mathbb{Y}}^2(u_{\mathbb{X}, \mathbb{Y}}^{\alpha_0})] \leq \|u_{\mathbb{X}, \mathbb{Y}}^{\alpha_0}\|_{\mathcal{H}_K}^2$$

thanks to the already established inequality for  $d_{\mathbb{X}, \mathbb{Y}}^2(u_{\mathbb{X}, \mathbb{Y}}^\alpha)$ . Finally, it holds that (along the same subsequence of above for which we do not introduce extra notation)

$$\|u_{\mathbb{X}, \mathbb{Y}}^0\|_{\mathcal{H}_K} = \|u_{\mathbb{X}, \mathbb{Y}}^\infty\|_{\mathcal{H}_K} \leq \liminf_{k \rightarrow \infty} \|u_{\mathbb{X}, \mathbb{Y}}^{\alpha_k}\|_{\mathcal{H}_K} \leq \limsup_{k \rightarrow \infty} \|u_{\mathbb{X}, \mathbb{Y}}^{\alpha_k}\|_{\mathcal{H}_K} \leq \|u_{\mathbb{X}, \mathbb{Y}}^0\|_{\mathcal{H}_K}$$

and all claims are established since convergence in a Hilbert space is equivalent to weak convergence and convergence of the norm and we proved that every sequence has a subsequence that converges to the same limit.  $\square$

**Remark 2.9.** *While the above discussion revolved around the use of a positive definite kernel, it is useful and instructive to consider two extreme cases: the Laplace and the Gauss kernels. They represent a minimally smooth kernel (not even continuously differentiable), and a maximally smooth one (analytic). The latter one delivers higher order (and correspondingly worse conditioned) methods, while the first helps mitigating the intrinsic ill-posedness of exact interpolation. A slightly regularized version of the Laplace kernel will be used in numerical calculations for this very reason. We also notice that, in [17], a derivation of Gauss kernel interpolation based on the use of the heat equation is proposed, which, at a purely formal level, amounts to replacing the Bessel potential norm in (2.2) and (2.3) by the much stronger norm*

$$\frac{1}{2} \|e^{-\Delta} u\|_{L^2}^2 = \frac{1}{2} \|e^{|\cdot|^2} \hat{u}\|_{L^2}^2.$$

While the use of arbitrary (positive definite) kernels is possible and useful, it sometimes obscures the exact nature of the differential operator that generates the norm on the reproducing kernel Hilbert space.

It is Remark 2.7 that lead us to interpret problems (2.2) and (2.3) as representing interpolation and approximate interpolation problems for functions  $f$  defined on a manifold  $\mathcal{M}$ , where  $\mathcal{M}$  is only known through the cloud/sample  $\mathbb{X}$  and  $f$  through the values  $\mathbb{Y}$  which coincide with  $f(\mathbb{X})$  or approximate it. In order to access geometric information about  $\mathcal{M}$  from  $\mathbb{X}$ , it is then natural to use  $u_{\mathbb{X},1}^\alpha$ , i.e. to choose  $f \equiv 1$ , as a proxy for a defining function (or at least a local level set function). In the rest of the paper, when performing numerical experiments, we shall make use of the Gauss kernel as well as the Laplace kernel, albeit in the regularized form  $L_\varepsilon(x) = e^{-\sqrt{|x|^2+\varepsilon}}$ ,  $x \in \mathbb{R}^n$ , when needed. The former is prototypical of many a very smooth kernel, while the second has minimal regularity and, even in its regularized form  $L_\varepsilon$ , significantly alleviates the ill-conditioning of the interpolation matrix as already mentioned above. Kernels of any intermediate regularity between these extreme cases are, e.g., those of the already mentioned Matérn family.

### 3. HYPERSURFACES

Given a point cloud or sample  $\mathbb{X}$  of a compact smooth hypersurface  $\mathcal{M}$ , we choose a kernel  $K$ , that is at least twice continuously differentiable and compute the function

$$u_{\mathbb{X}} = u_{\mathbb{X},1} = K(\cdot, \mathbb{X})K(\mathbb{X}, \mathbb{X})^{-1}\mathbb{1},$$

which amounts to a smooth extension of the constant function with value 1 from  $\mathbb{X}$  to the ambient space. As the kernel is known, differential quantities associated to this function can be computed analytically anywhere. Whenever  $[u_{\mathbb{X}} = 1]$  defines a hypersurface in the vicinity of one of its points, we can define the implied normal vector to this surface by

$$\nu_{\mathbb{X}}(x) = \frac{\nabla u_{\mathbb{X}}(x)}{|\nabla u_{\mathbb{X}}(x)|},$$

where, again, the only numerical computation is that of the coefficients  $K(\mathbb{X}, \mathbb{X})^{-1}\mathbb{1}$  since  $\nabla K(\cdot, \mathbb{X})$  can be computed exactly. Similarly one obtains

$$D\nu_{\mathbb{X}} = \frac{1}{|\nabla u_{\mathbb{X}}|}(D^2u_{\mathbb{X}} - D^2u_{\mathbb{X}}\nu_{\mathbb{X}}\nu_{\mathbb{X}}^T),$$

i.e., a numerical approximation for the derivative  $D\nu_{\mathbb{X}}$  of the normal in the spirit of meshfree methods. For stability reasons and/or in the presence of noise, one can replace  $u_{\mathbb{X}}$  by  $u_{\mathbb{X}}^\alpha = u_{\mathbb{X},1}^\alpha$  with a small  $\alpha > 0$  or one related to the noise level, if known. We shall revisit the choice of  $\alpha > 0$  for noisy data in the section where we address the connection to Gaussian Process Regression. The quantities  $\nu_{\mathbb{X}}$  and  $D\nu_{\mathbb{X}}$  will give us numerical access to the tangent plane to the surface as well as to its principal curvatures. This, in turn will open the door to the numerical computation of geometric operators acting on functions defined on  $\mathbb{X}$ . Notice that the deployment of  $u_{\mathbb{X},1}$  replaces the use of the more commonly encountered signed distance function (to the surface) which, however, would require knowledge of the normal in order to be properly interpolated. This is possible within the class of kernels chosen here that are peaked at their center. The approach also naturally offers a fix in the case of noisy data which consists in making the estimation of geometric quantities robust by turning on the regularization ( $\alpha > 0$ ). Estimates for the curvatures of a discrete surface are of interest in many applications. We refer to [9] for the case of smooth (polygonal) data and to [20] for the noisy case as well as to the references found in both for additional context.

**3.1. Interpolation Results.** It was observed in [13] that the restriction of full space positive definite kernels  $K$  to a smooth compact embedded submanifold  $\mathcal{M} \subset \mathbb{R}^d$  without boundary of any dimension is itself a positive kernel  $K_{\mathcal{M}} : \mathcal{M} \times \mathcal{M} \rightarrow \mathbb{R}$ . They also identify the corresponding native space of functions over  $\mathcal{M}$  for kernels of known finite smoothness and derive Sobolev error estimates for the interpolation problem for functions defined on  $\mathcal{M}$ . Here we take a more direct approach to reach the same conclusion. In essence, when  $\mathbb{X}$  happens to be a sample of a smooth manifold with the above properties, the full space interpolant  $u_{\mathbb{X}, \mathbb{Y}}$  can be interpreted as a function in  $\mathcal{H}_K$ , the trace  $\gamma_{\mathcal{M}}(u_{\mathbb{X}, \mathbb{Y}})$  of which is an interpolant for  $u : \mathcal{M} \rightarrow \mathbb{R}$  corresponding to the data  $(\mathbb{X}, \mathbb{Y})$ . Notice that, as long as  $K$  has at least the regularity of the Laplace kernel  $L$ , this approach makes sense since the corresponding native space is contained in  $H^{\frac{d+1}{2}}(\mathbb{R}^d) \hookrightarrow \text{BUC}(\mathbb{R}^d)$ . Thus full space interpolation of data living on a manifold naturally leads to approximations of functions belonging to the trace space of the native space. This is in line with the results of [13] and offers a slightly different point of view. A difference between this paper and [13] is that we are also interested in using the data  $\mathbb{X}$  to interpolate the manifold itself in order to be able to derive approximations for its geometric quantities and operators. This is the main reason why we prefer to still think in terms of full space kernel interpolation: defining functions of  $\mathcal{M}$  do indeed live in full space. We also observe that the minimally smooth case of the Laplace kernel opens the door to effectively dealing with non-smooth manifolds as the level sets of  $H^{\frac{d+1}{2}}(\mathbb{R}^d)$  functions do not enjoy much regularity. With the use of regularization ( $\alpha > 0$ ), the method can also be made robust even in the presence of noise.

**Remark 3.1.** *We point out that, even in the minimally smooth case of the Laplace kernel, when working in the context of a low regularity submanifold  $\mathcal{M}$ , the level set function  $u_{\mathbb{X}, 1}$  is minimally smooth merely on  $\mathcal{M}/\mathbb{X}$  as it holds that  $\mathcal{A}_K u_{\mathbb{X}, 1} = 0$  away from  $\mathcal{M}/\mathbb{X}$ , showing that  $u_{\mathbb{X}, \mathbb{Y}} \in \text{dom}(\tilde{\mathcal{A}}_K^n)$  for every  $n \in \mathbb{N}$ , where  $\tilde{\mathcal{A}}_K$  is the restriction of  $\mathcal{A}_K$  to the open set  $\mathcal{M}^c/\mathbb{X}^c$ . Thus, in particular, the level sets other than the one with value 1 are typically smoother. This makes it possible to compute approximate values for geometric quantities even when the kernel lacks the necessary regularity.*

Let  $u \in H^m(\mathbb{R}^d)$  for  $m > \frac{d}{2}$  be an arbitrary function with  $u = f$ , where  $f \in H^{m-1/2}(\mathcal{M})$  is given and  $\mathcal{M}$  is assumed to be either a compact smooth hypersurface without boundary in  $\mathbb{R}^d$  or a finite set  $\mathbb{X} \subset \mathcal{M}$ . The minimizer of an  $H^m(\mathbb{R}^d)$ -norm functional  $E_m$  such as

$$E_m(u) = \frac{1}{2} \|u\|_{H^m(\mathbb{R}^d)}^2$$

with the constraint  $u = f$  on  $\mathcal{M}$  is a relevant example in our context. When  $\mathcal{M}$  is a manifold, the minimizer is denoted by  $u_{\mathcal{M}, f}$  in line with the notation used previously in the case when  $\mathcal{M} = \mathbb{X}$ ,  $f = \mathbb{Y}$ . Notice that, since  $m > \frac{d}{2}$ , pointwise evaluations are possible and that the trace theorem ensures that  $\{u \in H^m(\mathbb{R}^d) \mid u = f \text{ on } \mathcal{M}\} \neq \emptyset$ . We are particularly interested in the case when  $\mathbb{Y} = f(\mathbb{X})$ , which makes sense since the evaluation of  $f$  is possible as  $m - \frac{1}{2} > \frac{d-1}{2}$  by assumption. The minimizers  $u_{\mathcal{M}, f}$  and  $u_{\mathbb{X}, f(\mathbb{X})} = u_{\mathbb{X}, \mathbb{Y}}$ , with  $\mathbb{Y} = f(\mathbb{X}) = \gamma_{\mathcal{M}}(u)(\mathbb{X})$ , both exist since the convex set determined by the constraint is non-empty and both belong to  $H^m(\mathbb{R}^d)$ . Thus it holds that

$$u_{\mathbb{X}, \mathbb{Y}}|_{\mathcal{M}} \in H^{m-1/2}(\mathcal{M}) \text{ and } u_{\mathbb{X}, \mathbb{Y}}|_{\mathcal{M}}(\mathbb{X}) = f(\mathbb{X})$$

It follows that the function  $u_{\mathbb{X}, \mathbb{Y}}|_{\mathcal{M}} - f$  vanishes on  $\mathbb{X} \subset \mathcal{M}$ . We can therefore use results about the behavior of Sobolev functions with scattered zeros as they can be found in [3] for  $\frac{d}{2} < m \in \mathbb{N}$ , or in [34] for  $m \in (\frac{d}{2}, \infty) \setminus \mathbb{N}$ . While the results hold in the general context of  $p \in [1, \infty)$ , we shall work with  $p = 2$  and  $m > \frac{d}{p} = \frac{d}{2}$ , when it holds that

$$|u|_{H^k(\Omega)} \leq c h_{\mathbb{X}, \Omega}^{m-k} |u|_{H^m(\Omega)} \text{ and } \|u\|_{\infty} \leq c h_{\mathbb{X}, \Omega}^{m-d/2} |u|_{H^m(\Omega)}, \quad (3.1)$$

for  $u \in H^m(\Omega)$  with  $u(\mathbb{X}) \equiv 0$  on the assumption that  $\Omega$  satisfy a geometric property which always holds for balls and where  $h_{\mathbb{X}, \Omega}$  is the so-called fill-distance of  $\mathbb{X}$  given by

$$h_{\mathbb{X}, \Omega} = \sup_{x \in \Omega} \min_{\tilde{x} \in \mathbb{X}} |x - \tilde{x}|.$$

It is a measure of how the set  $\mathbb{X}$  approximates  $\Omega$ . The norms appearing in the estimate are the semi-norms for the Beppo Levi spaces  $BL_k = \{u \in \mathcal{D}'(\Omega) \mid \partial^\alpha u \in L_2(\Omega) \ \forall |\alpha| = k\}$  given by

$$|u|_{H^k(\Omega)}^2 = \sum_{|\alpha|=k} \|\partial^\alpha u\|_2^2.$$

They are norms when  $k > \frac{d}{2}$ . The result is based on local polynomial approximation. Transferring this result to the hypersurface  $\mathcal{M}$  yields the theorem below.

**Remark 3.2.** Notice that that a more general result for Sobolev norms is formulated and proved in [13] which allows  $\mathcal{M}$  to be a submanifold of any dimension and the regularity to be fractional as well. Here we only provide a brief sketch of the proof specifically designed for our context for the sake of completeness. While formulated for hypersurfaces, it carries over verbatim to the case of submanifolds of any dimension.

**Theorem 3.3.** Let  $\mathcal{M} \subset \mathbb{R}^d$  be a smooth compact hypersurface and  $f \in H^{m-1/2}(\mathcal{M})$  be given with  $m > \frac{d}{2}$ . Let  $\mathbb{X} \subset \mathcal{M}$  and

$$h_{\mathbb{X}, \mathcal{M}} = \sup_{x \in \mathcal{M}} \min_{\tilde{x} \in \mathbb{X}} d_{\mathcal{M}}(x, \tilde{x})$$

be the fill distance of the set  $\mathbb{X}$  for the manifold  $\mathcal{M}$ . If  $f(\mathbb{X}) \equiv 0$ , then it holds that

$$|f|_{H^k(\mathcal{M})} \leq c h_{\mathbb{X}, \mathcal{M}}^{m-1/2-k} |f|_{H^{m-1/2}(\mathcal{M})} \text{ and } \|f\|_\infty \leq c h_{\mathbb{X}, \mathcal{M}}^{m-d/2} |f|_{H^{m-1/2}(\mathcal{M})}.$$

*Proof.* As  $\mathcal{M}$  is assumed to be compact, it is possible to find a finite number of open chart domains  $U_j \subset \mathcal{M}$ ,  $j = 1, \dots, J$ , and (bijective) charts (local coordinates)

$$\varphi_j : U_j \rightarrow \mathbb{B}_{\mathbb{R}^{d-1}}(0, 1),$$

such that  $\varphi_j^{-1} : \mathbb{B}_{\mathbb{R}^{d-1}}(0, 1) \rightarrow \mathbb{R}^d$  is smooth and  $\varphi_j^{-1}(\mathbb{B}_{\mathbb{R}^{d-1}}(0, 1)) = \mathcal{M} \cap U_j = U_j$ . Choosing a smooth partition of unity  $\{\psi_j : \mathcal{M} \rightarrow \mathbb{R} \mid j = 1, \dots, J\}$  subordinate to this cover by chart domains, it is possible to obtain an (equivalent) norm on  $H^{m-1/2}(\mathcal{M})$  given by

$$\|v\|_{H^{m-1/2}(\mathcal{M})} \sim \left( \sum_{j=1}^J \|(v\psi_j) \circ \varphi_j^{-1}\|_{H^{m-1/2}(\mathbb{B}_{\mathbb{R}^{d-1}(0,1)})}^2 \right)^{1/2},$$

where  $v \in H^{m-1/2}(\mathcal{M})$ . Next define  $\mathbb{X}_j = \mathbb{X} \cap U_j$  and  $\mathbb{Z}_j = \varphi_j(\mathbb{X}_j)$  for  $j = 1, \dots, J$ . It holds that

$$h_{\mathbb{Z}_j, \mathbb{B}_{\mathbb{R}^{d-1}(0,1)}} = \sup_{z \in \mathbb{B}_{\mathbb{R}^{d-1}(0,1)}} \min_{\tilde{z} \in \mathbb{Z}_j} |z - \tilde{z}| = \sup_{x \in U_j} \min_{\tilde{x} \in \mathbb{X}_j} |\varphi_j(x) - \varphi_j(\tilde{x})| \leq c_j h_{\mathbb{X}_j, U_j} \leq c h_{\mathbb{X}, \mathcal{M}},$$

where  $h_{\mathbb{Z}_j, \mathbb{B}_{\mathbb{R}^{d-1}(0,1)}}$  is the corresponding fill distance for  $\mathbb{Z}_j$  in  $\mathbb{B}_{\mathbb{R}^{d-1}(0,1)}$ . The last inequality can be obtained as follows: we can assume without loss of generality that the sets  $U_j$  are geodesic balls centered at  $p_j$  and with radii  $r_j$  as well as that  $h_{\mathbb{X}, \mathcal{M}} < \min_{j=1, \dots, J} r_j$ . Then, if  $x \in \mathbb{B}_{\mathcal{M}}(p_j, r_j - h_{\mathbb{X}, \mathcal{M}})$ , we can find  $\tilde{x} \in \mathbb{X}$  such that  $d(x, \tilde{x}) \leq h_{\mathbb{X}, \mathcal{M}}$ , in which case  $\tilde{x} \in \mathbb{X}_j$ . Else, if  $r_j - h_{\mathbb{X}, \mathcal{M}} \leq d_{\mathcal{M}}(x, p_j) < r_j$ , we can find a point  $\bar{x}$  along the geodesic connecting  $p_j$  to  $x$  with  $d(p_j, \bar{x}) = r_j - h_{\mathbb{X}, \mathcal{M}}$  and  $\tilde{x} \in \mathbb{X}_j$  with  $d(\bar{x}, \tilde{x}) \leq h_{\mathbb{X}, \mathcal{M}}$ , in which case we have

$$d_{\mathcal{M}}(x, \tilde{x}) \leq d_{\mathcal{M}}(x, \bar{x}) + d_{\mathcal{M}}(\bar{x}, \tilde{x}) \leq r_j - (r_j - h_{\mathbb{X}, \mathcal{M}}) + h_{\mathbb{X}, \mathcal{M}} \leq 2h_{\mathbb{X}, \mathcal{M}}.$$

Notice that  $|\mathbb{X}_j| = |\mathbb{Z}_j|$  since  $\varphi_j$  is bijective and that

$$\begin{aligned} h_{\mathbb{X}_j, U_j} &= \sup_{x \in U_j} \inf_{\tilde{x} \in \mathbb{X}_j} d_{\mathcal{M}}(x, \tilde{x}) = \sup_{z \in \mathbb{B}_{\mathbb{R}^{d-1}(0,1)}} \inf_{\tilde{z} \in \mathbb{Z}_j} d_{\mathcal{M}}(\varphi^{-1}(z), \varphi^{-1}(\tilde{z})) \\ &\leq c \sup_{z \in \mathbb{B}_{\mathbb{R}^{d-1}(0,1)}} \inf_{\tilde{z} \in \mathbb{Z}_j} |z - \tilde{z}| = c h_{\mathbb{Z}_j, \mathbb{R}^{d-1}(0,1)}. \end{aligned}$$

An application of (3.1) for each  $j = 1, \dots, J$ , yields

$$\|(f\psi_j) \circ \varphi_j^{-1}\|_{H^k(\mathbb{B}_{\mathbb{R}^{d-1}(0,1)})} \leq c_j h_{\mathbb{Z}_j, H^k(\mathbb{B}_{\mathbb{R}^{d-1}(0,1)})}^{m-1/2-k} \|(f\psi_j) \circ \varphi_j^{-1}\|_{H^{m-1/2}(\mathbb{B}_{\mathbb{R}^{d-1}(0,1)})}$$

and

$$\|(f\psi_j) \circ \varphi_j^{-1}\|_{\infty} \leq c_j h_{\mathbb{Z}_j, H^k(\mathbb{B}_{\mathbb{R}^{d-1}(0,1)})}^{m-1/2-(d-1)/2} \|(f\psi_j) \circ \varphi_j^{-1}\|_{H^{m-1/2}(\mathbb{B}_{\mathbb{R}^{d-1}(0,1)})},$$

and the claim follows by combining these inequalities and using the relation between the fill distance on the manifold to that in coordinate balls.  $\square$

**Corollary 3.4.** *Define  $u_{\mathbb{X}, f(\mathbb{X})}$  to be the minimizer of the  $H^m(\mathbb{R}^d)$ -norm subject to the constraint that  $u_{\mathbb{X}, f(\mathbb{X})}(\mathbb{X}) = f(\mathbb{X})$ . Then the function*

$$u_{\mathbb{X}, f(\mathbb{X})}|_{\mathcal{M}} - f \in H^{m-1/2}(\mathcal{M})$$

vanishes on  $\mathbb{X}$  and it holds that

$$\|u_{\mathbb{X}, f(\mathbb{X})}|_{\mathcal{M}} - f\|_{H^k(\mathcal{M})} \leq c h_{\mathbb{X}, \mathcal{M}}^{m-1/2-k} \|u_{\mathbb{X}, f(\mathbb{X})}|_{\mathcal{M}} - f\|_{H^{m-1/2}(\mathcal{M})}.$$

as well as

$$\|u_{\mathbb{X}, f(\mathbb{X})}|_{\mathcal{M}} - f\|_{\infty} \leq c h_{\mathbb{X}, \mathcal{M}}^{m-d/2} \|u_{\mathbb{X}, f(\mathbb{X})}|_{\mathcal{M}} - f\|_{H^{m-1/2}(\mathcal{M})}.$$

Furthermore, since  $u_{\mathbb{X}, f(\mathbb{X})}$  and  $u_{\mathcal{M}, f}$  are  $H^m(\mathbb{R}^d)$ -extensions of  $u_{\mathbb{X}, f(\mathbb{X})}|_{\mathcal{M}}$  and  $f$  with continuous dependence by construction, it also holds that

$$\|u_{\mathbb{X}, f(\mathbb{X})} - u_{\mathcal{M}, f}\|_{H^{k+1/2}(\mathbb{R}^d)} \leq c h_{\mathbb{X}, \mathcal{M}}^{m-1/2-k} \|u_{\mathbb{X}, f(\mathbb{X})}|_{\mathcal{M}} - f\|_{H^{m-1/2}(\mathcal{M})}.$$

In kernel interpolation it is sometimes the case that one uses a positive definite kernel  $K : \Omega \times \Omega \rightarrow \mathbb{R}$ ,  $\Omega \subset \mathbb{R}^d$ , without an explicit characterization of the associated native space  $\mathcal{H}_K$ . As we saw earlier,  $u_{\mathbb{X}, \mathbb{Y}} = K(\cdot, x)K(\mathbb{X}, \mathbb{X})^{-1}\mathbb{Y}$  is an interpolant for the values  $\mathbb{Y} \subset \mathbb{R}^{|\mathbb{X}|}$  at the arguments  $\mathbb{X} \subset \Omega$  and has minimal  $\mathcal{H}_K$ -norm among all interpolants. Estimates for functions with scattered zeros like the above in that context can then be derived as soon as one knows that  $\mathcal{H}_K \hookrightarrow H^m(\Omega)$ . Thus the estimates obtained above can also be used for e.g. Gauss kernel  $G$  provided  $f$  is a smooth enough function ensuring solvability of the interpolation problem. This is due to the fact that  $\mathcal{H}_G \hookrightarrow H^m(\mathbb{R}^d)$  for every  $m \in \mathbb{N}$ . As the Gauss kernel is analytic, when the manifold and the data are analytic, one would expect even better convergence results along the lines of [34, Section 11.4].

If one is only interested in  $\mathcal{M}$  and its geometry, then  $f \equiv 1$  and the estimates are available on appropriate regularity assumptions on  $\mathcal{M}$  only. While the above theoretical results are clearly valid for the Laplace kernel, its lack of smoothness does not allow for high order approximations. Numerical experiments will show that high order can be recovered by switching to the regularized kernel  $L_{\varepsilon}$  mentioned before while, simultaneously, curbing the ill-posedness of the system somewhat.

**Remark 3.5.** *Kernel interpolation can deliver high order methods but, inevitably, this comes at the cost of ill-posedness. The latter, in turn, used to be thought of as a limitation to the size of point clouds that could be considered. It has since been observed that the use of compactly supported radial basis functions [25, 26], the use of the Multipole Method with smooth kernel functions [4, 5], or the use of the partition of unity method [35] can effectively mitigate this shortcoming.*

**Remark 3.6.** *Kernel methods on special manifolds are also considered in the literature (see for instance [34]) following an approach based on kernels that live on the manifold itself and are related to its geometry. As explicit kernels are only known for very special manifolds, this leads to natural limitations.*

**3.2. Computation of Geometric Quantities.** Next we consider the problem of computing a numerical approximation to the surface gradient  $\nabla_{\mathcal{M}} f$  and the Laplace Beltrami  $\Delta_{\mathcal{M}} f$  operator of a function  $f : \mathcal{M} \rightarrow \mathbb{R}$  defined on a smooth compact hypersurface  $\mathcal{M}$ . This is a problem of general interest due to its manifold applications: surface fairing/smoothing/denoising, feature detection, mesh optimization and simplification, geometric compression, shape analysis and recognition, 3D reconstruction, registration of surfaces, medical imaging, surface based morphology, rendering, and PDEs on manifolds. It has been widely studied in the literature in the context of various discrete representations of surfaces (see for instance [31, 23]). It was also considered for radial basis functions representations [27]. As mentioned before, however, the accepted approach is that of augmenting the data set  $\mathbb{X}$  with two equidistant layers of additional points  $\mathbb{X} \pm \delta \nu_{\mathcal{M}}(\mathbb{X})$  located at a distance  $\delta > 0$  from  $\mathbb{X}$  in direction of the positive and negative normals\* and impose values at these points in an effort to make the interpolant be an approximation of a “signed distance function” for the manifold sampled by  $\mathbb{X}$ . The appearance of disconnected components in the level sets of the interpolant along with added stability are often adduced as the reasons justifying the need of such an augmentation [27]. We believe (and will show evidence in the last section) that disconnections are caused by the use of very smooth (analytic) kernels, which, by design, try to interpolate sparse, less smooth, or noisy hypersurfaces by highly regular functions, which tend to use complex multi-component level sets so as to accommodate the sample while maintaining regularity. We will show that the use of low regularity (or close to such) kernels and/or regularization in the sense advocated here (via regression) can fix this problem. It should also be mentioned that some knowledge of the normal to the surface is required in order to effectively implement an augmentation strategy. Additionally, exogenus parameters are introduced that affect the approximation quality and the conditioning of the resulting systems. These parameters also need to be determined somehow. While accuracy is lost (short of exact knowledge of the normals), this approach reduces the computation of geometric operators to the computation of ambient space operators applied to ambient space functions obtained by constant extension in normal direction to the off-surface points (see e.g. [27]).

We assume again that  $\mathcal{M}$  is known only through a sample  $\mathbb{X} \subset \mathcal{M}$  of its points and that the values of  $f$  are only available for  $\mathbb{X}$ , i.e. we assume  $f(\mathbb{X}) = \mathbb{Y}$  to be known. The starting point is the ability that we have gained of obtaining geometric information about a hypersurface from a discrete sample of its points via the associated signature function  $u_{\mathbb{X}}$ . The algorithm is based on performing computations on the interpolant  $u_{\mathbb{X}, \mathbb{Y}}$  that is viewed as an approximation to the extension  $u_{\mathcal{M}, f}$  of  $f$  to the whole space. We therefore need to derive a formula for the surface operators in terms of the embedding  $\mathcal{M} \subset \mathbb{R}^d$  (or in terms of  $\mathbb{X}$ ) that we can apply to the extension and then consider appropriate “discrete” counterparts. As we were not able to find a such formula for the Laplace-Beltrami operator in the standard differential geometry textbooks, we give a brief derivation here.

**Definition 3.7.** *Let  $U, V : \mathcal{M} \rightarrow T\mathcal{M}$  be smooth sections of the tangent bundle (i.e. vector fields on  $\mathcal{M}$ ). Then  $D_V$  denotes the derivative along the vector field  $V$ , i.e.*

$$D_V f(x) = \left. \frac{d}{dt} \right|_{t=0} f(\varphi_V(t, x)), \quad D_V U(x) = \left. \frac{d}{dt} \right|_{t=0} U(\varphi_V(t, x)), \quad x \in \mathcal{M},$$

where  $\varphi_V(t, \cdot)$  is the flow generated by  $V$ , i.e. it solves the ordinary differential equation

$$\begin{cases} \dot{\gamma} = V(\gamma), & t > 0, \\ \gamma(0) = x \end{cases}$$

---

\*Since [19], the normals are typically approximated by Principal Component Analysis estimation of the tangent plane based on a ( $k$ )-nearest neighbors vicinity of each point.

where  $\gamma : [0, \infty) \rightarrow \mathcal{M}$  is a curve on  $\mathcal{M}$ . This is well-defined since  $V(x) \in T_x \mathcal{M}$  for every  $x \in \mathcal{M}$ . Even if  $U$  is a tangential vector field, it will in general not hold that  $D_V U(x) \in T_x \mathcal{M}$ . This motivates the definition of the covariant derivative (connection)

$$\nabla_V U = \partial_V U = D_V U - (\nu \cdot D_V U) \nu,$$

obtained by applying the orthogonal projection  $\mathbb{1}_d - \nu \nu^\top$  onto the tangent space  $T\mathcal{M}$  of  $\mathcal{M}$  to the directional derivative  $D_V U$ .

Now take  $u_{\mathcal{M},f} : \mathbb{R}^d \rightarrow \mathbb{R}$  or any other (smooth) extension of the function  $f : \mathcal{M} \rightarrow \mathbb{R}$  of interest. Then it holds that

$$\nabla_{\mathcal{M}} u(y) = \nabla u(y) - (\nu_{\mathcal{M}}(y) \cdot \nabla u(y)) \nu_{\mathcal{M}}(y),$$

where  $\nabla = \nabla_{\mathbb{R}^d}$  is the canonical gradient in the ambient space. In order to compute the Laplace-Beltrami operator for  $\mathcal{M}$

$$\Delta_{\mathcal{M}} = \operatorname{div}_{\mathcal{M}} \nabla_{\mathcal{M}}$$

in terms of the coordinates of the ambient space  $\mathbb{R}^d$ , we need the following lemma.

**Lemma 3.8.** *For a smooth function  $u : \mathbb{R}^d \rightarrow \mathbb{R}$  it holds that*

$$\Delta_{\mathcal{M}} u(x) = \operatorname{tr}(D^2 u(x)) - \nu(x)^\top D^2 u(x) \nu(x) + (d-1)H(x) \partial_\nu u(x), \quad x \in \mathcal{M}.$$

*Proof.* If  $X : \mathcal{U} \rightarrow \mathbb{R}^{d-1}$  is a local coordinate system for  $\mathcal{M}$  about a point  $y \in \mathcal{M}$ , then the tangent space is spanned by the vectors

$$\frac{\partial}{\partial x^j} = \left( \frac{\partial}{\partial x^j} X^{-1} \right)(X(y)), \quad j = 1, \dots, d-1,$$

where it is typically assumed that  $X(y) = 0$  when working in a neighborhood  $\mathcal{U}$  of  $y$ . It follows that

$$\nabla_{\frac{\partial}{\partial x^j}} \frac{\partial}{\partial x^k} = \frac{\partial}{\partial x^j} \frac{\partial}{\partial x^k} - \left( \frac{\partial}{\partial x^j} \frac{\partial}{\partial x^k} \cdot \nu \right) \nu,$$

but  $\frac{\partial}{\partial x^k} \cdot \nu = 0$  and thus

$$\frac{\partial}{\partial x^j} \frac{\partial}{\partial x^k} \cdot \nu = - \frac{\partial}{\partial x^j} \nu \cdot \frac{\partial}{\partial x^k}.$$

It follows that

$$\nabla_{\frac{\partial}{\partial x^j}} \frac{\partial}{\partial x^k} = \frac{\partial}{\partial x^j} \frac{\partial}{\partial x^k} + \frac{\partial}{\partial x^k} \cdot \frac{\partial}{\partial x^j} \nu = \frac{\partial}{\partial x^j} \frac{\partial}{\partial x^k} + \frac{\partial}{\partial x^j} \cdot \frac{\partial}{\partial x^k} \nu,$$

where the last identity follows from  $\frac{\partial}{\partial x^j} \cdot \nu = 0$  in view of the commutativity of the regular derivatives and hence from

$$\frac{\partial}{\partial x^k} \cdot \left( \frac{\partial}{\partial x^j} \nu \right) = - \frac{\partial}{\partial x^k} \frac{\partial}{\partial x^j} \cdot \nu = \frac{\partial}{\partial x^j} \cdot \left( \frac{\partial}{\partial x^k} \nu \right).$$

Summarizing we obtain that

$$\nabla_{\frac{\partial}{\partial x^j}} \nabla_{\frac{\partial}{\partial x^k}} u = \nabla_{\frac{\partial}{\partial x^j}} \frac{\partial}{\partial x^k} u = \frac{\partial}{\partial x^j} \frac{\partial}{\partial x^k} u + \left( \frac{\partial}{\partial x^j} \cdot \frac{\partial}{\partial x^k} \nu \right) \partial_\nu u.$$

Now, take a system of local coordinates that yields an orthonormal basis at  $y$  for the tangent space. Observe that the addition of  $\nu(y)$  extends it to an orthonormal basis of  $\mathbb{R}^d$ , so that, taking a trace in these coordinates at  $y$ , we arrive at

$$\begin{aligned} \Delta_{\mathcal{M}} u &= \nabla_{\frac{\partial}{\partial x^j}} \nabla_{\frac{\partial}{\partial x^j}} u = \frac{\partial}{\partial x^j} \frac{\partial}{\partial x^j} u + \left( \frac{\partial}{\partial x^j} \cdot \frac{\partial}{\partial x^j} \nu \right) \partial_\nu u \\ &= \operatorname{tr}(D^2 u) - \nu^\top D^2 u \nu + (d-1)H \partial_\nu u, \end{aligned} \tag{3.2}$$

(where the summation convention was used) noticing that the mean curvature  $H$  satisfies

$$(d-1)H = \operatorname{tr}(D\nu),$$

since  $\partial_\nu \nu = 0$ . □

In order to obtain a viable numerical algorithm, it remains only to compute the interpolants  $u_{\mathbb{X}}$  and  $u_{\mathbb{X},\mathbb{Y}}$  corresponding to the data set  $(\mathbb{X}, \mathbb{Y})$ . The first is used in order to compute the implied normal  $\nu_{\mathbb{X}}$  and the implied mean curvature  $H_{\mathbb{X}} = \frac{1}{d-1} \text{tr}(D\nu_{\mathbb{X}})$  as described before, whereas the second yields a smooth extension of  $f|_{\mathbb{X}}$  to the full ambient space that is a numerical approximation of the extension  $u_{\mathcal{M},f} : \mathbb{R}^d \rightarrow \mathbb{R}$  of  $f$  as explained in the previous subsection. Then, the formulæ for surface gradient and Laplace-Beltrami operators immediately yield numerical discretizations given by

$$\nabla_{\mathbb{X}} \mathbb{Y} = \nabla_{\mathbb{X}} u_{\mathbb{X},\mathbb{Y}} = \nabla u_{\mathbb{X},\mathbb{Y}} - (\nabla u_{\mathbb{X},\mathbb{Y}} \cdot \nu_{\mathbb{X}}) \nu_{\mathbb{X}},$$

and

$$\Delta_{\mathbb{X}} \mathbb{Y} = \Delta_{\mathbb{X}} u_{\mathbb{X},\mathbb{Y}} = \text{tr}(D^2 u_{\mathbb{X},\mathbb{Y}}) - \nu_{\mathbb{X}}^\top D^2 u_{\mathbb{X},\mathbb{Y}} \nu_{\mathbb{X}} + (d-1) H_{\mathbb{X}} \nabla u_{\mathbb{X},\mathbb{Y}} \cdot \nu_{\mathbb{X}},$$

where all derivatives involved are computed analytically. These expressions can be evaluated anywhere as they are combinations of functions defined everywhere. Matrix discretizations are obtained by evaluating the expressions  $\nabla_{\mathbb{X}} \mathbb{Y}$  and  $\Delta_{\mathbb{X}} \mathbb{Y}$  at  $\mathbb{X}$ . It is also possible to obtain non square representations evaluating at other discrete sets  $\tilde{\mathbb{X}}$  and/or to replace the “grid”  $\mathbb{X}$  by substituting  $\mathbb{Y}$  with  $u_{\mathbb{X},\mathbb{Y}}(\tilde{\mathbb{X}})$  to arrive at matrices that approximate the operators and take inputs defined on  $\tilde{\mathbb{X}}$  and produce outputs defined on that same grid.

#### 4. CONNECTION TO REGRESSION

Before moving on to numerical experiments, we address the connection to Gaussian Process Regression which yields an interpretation of the regularization parameter  $\alpha > 0$ .

**Definition 4.1.** *If  $E = E(\Omega) \subset C(\Omega)$  is a Banach space of functions, a random vector  $W \in E$  is said to have Gaussian law if  $e^* W = \langle e^*, W \rangle_{E^*, E}$  is normally distributed for each  $e^* \in E^*$ . It is called centered iff  $\mathbb{E}[e^* W] = 0$  for each  $e^* \in E^*$ .*

Multivariate Gaussian random variables on  $\mathbb{R}^d$  are the finite dimensional counterpart. The associated covariance function is given by

$$K(x, \tilde{x}) = \mathbb{E}[W(x)W(\tilde{x})], \quad x, \tilde{x} \in E,$$

and uniquely determines the law of the centered Gaussian random element. It is naturally non-negative definite as

$$0 \leq \mathbb{E}\left(\left[\sum_{i=1}^m a_i W(x_i)\right]^2\right) = \sum_{i,j=1}^m a_i a_j \mathbb{E}[W(x_i)W(x_j)] = \sum_{i,j=1}^n a_i a_j K(x_i, x_j) = a^\top K(\mathbb{X}, \mathbb{X}) a,$$

for any  $\mathbb{X} \subset \Omega$ . Thus one can start with a positive definite kernel  $K : \mathbb{R}^d \times \mathbb{R}^d \rightarrow \mathbb{R}$  and obtain an associated Gaussian random vector  $W \in C(\Omega)$ . When confronted with a data set  $(\mathbb{X}, \mathbb{Y})$  with  $\mathbb{X} \subset \Omega$  one can make the assumption that

$$y = f(x) + \varepsilon$$

where  $f \sim N(0, K)$ , i.e. one can use a prior for  $f$  in the form of a random function with vanishing mean and covariance function  $K$  and model the presence of noise by the additive white noise term  $\varepsilon$  (independent of  $f$ ) of variance  $\sigma^2 > 0$ . Given a value set  $\mathbb{Y}$  for a set of arguments  $\mathbb{X} \in \Omega$ , one can then try to compute the conditional value  $Y$  at a new argument  $x \in \Omega$  given the observed data

$$y|(x, f(\mathbb{X}) = \mathbb{Y}).$$

It is known, using standard properties of multivariate Gaussian distributions under conditioning and sum, that, on the above assumptions, the random variable  $Y$  is also Gaussian and that its expected value can be computed as

$$\mathbb{E}[Y] = K(x, \mathbb{X}) [\sigma^2 + K(\mathbb{X}, \mathbb{X})]^{-1} \mathbb{Y},$$

which is the exact kernel interpolation formula when  $\sigma = 0$  and coincides with the approximate interpolation formula when one chooses  $\alpha = \sigma^2 > 0$ . Thus one can think of the amount of regularization needed to be given by the amount of uncertainty in the data, if it is known. This also shows that the

choice of prior in Gaussian Process Regression, i.e. the choice of correlation function, determines the regularity properties of the approximate interpolant (i.e. the expectation of the posterior).

**Remark 4.2.** *An introduction to the statistical point of view of Gaussian Process Regression is a topic covered e.g. in the online book [28] in the context of Machine Learning. For the above problem it is also possible to determine the variance of  $Y$  which is given by*

$$\mathbb{E}[|Y - \mathbb{E}[Y]|^2] = K(x, x) + \sigma^2 - K(x, \mathbb{X})[\sigma^2 + K(\mathbb{X}, \mathbb{X})]^{-1}K(\mathbb{X}, x).$$

We refer to [28] for the material necessary to fill the gaps in the arguments of this section.

## 5. NUMERICAL EXPERIMENTS

**Remark 5.1.** *While the signature function is almost always a defining function, at least locally, there are circumstances in which it is not. Interestingly, this is the case when the curvature vanishes in the case of curves, and when the mean curvature vanishes for surfaces. These are all situations when the local symmetries of the manifold make the normal vector “vanish analytically” (as explained in the example below) and almost vanish numerically. In the next subsection we show that this is only the case in the absence of global information and does therefore not preclude the use of the method in the presence of some flatness.*

**5.1. Curves.** In this section we illustrate how the method performs on closed curves. In all figures, unless otherwise stated, we use white dots to indicate the data set  $\mathbb{X}$ , a red line to indicate the level 1 of the signature function  $u_{\mathbb{X}}$ , shades of green for its level regions, and black arrows for the implied normals  $\nu_{\mathbb{X}}$ . We begin by finishing the above discussion. We take a closed smooth curve  $\Gamma \subset \mathbb{R}^2$  parametrized by

$$(\sin(t), \sin^3(t) + .5 \cos(t)), t \in [0, 2\pi),$$

which has two inflection points. Figure 1 (left) shows the information recovered from  $u_{\mathbb{X}}$  where  $\mathbb{X}$

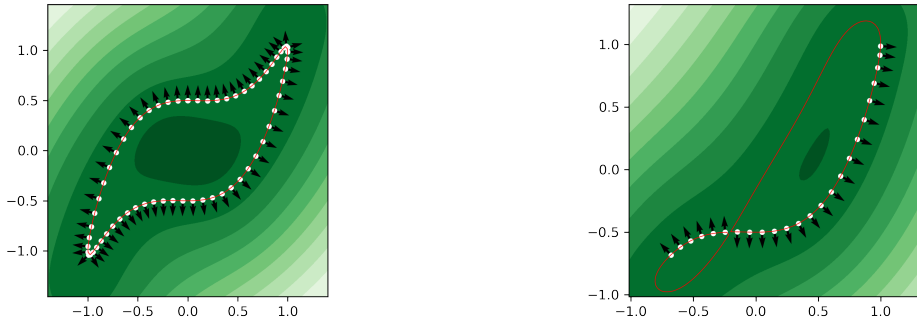


FIGURE 1. Reconstruction of a closed curve from 64 of its points (in white) on the left. Reconstruction based on an incomplete subsample consisting of 24 points on the right.

consists of 64 points at equidistant parameter values. As you can see the normals all point in an outward direction orthogonal to the curve. However, if we remove a part of the closed curve, it obviously becomes impossible to define regions interior and exterior to the curve and this is reflected in the vanishing of the gradient of  $u_{\mathbb{X}}$  at the one inflection point found on this portion of the curve as can be inferred from Figure 1 (right). As it is to be expected from the construction of  $u_{\mathbb{X}}$ , the induced normal, when computed based on local information alone, points in the direction of the region from which the curve looks (locally) convex (and thus effectively flips its sense as it goes through the inflection point as if using a discontinuous parametrization). In this example we used interpolation

with the Laplace kernel and  $\varepsilon = 1$ . Notice as well that the use of a smooth kernel still yields a smooth closed curve that is necessarily the level set of an analytic function.

Next we consider a non-smooth curve, a triangle. This example shows that, while the Gaussian kernel can be used also for samples of (simple) non-smooth curves, it will (as in the previous example) generate complicated level lines so as to decompose the curve into smooth pieces. The use of the Laplace kernel avoids this issue since the signature function on the set or its sample is only Hölder and can therefore easily accommodate abrupt turns in the curve. Even in more complicated non-smooth examples, Gauss interpolation yields complicated and mostly useless level sets but, at the same time, still delivers useful normals on the sample set as in the example of the triangle. Figure 2 shows the results for the Gauss (left) and Laplace (right) kernels, where 48 sample points are used and  $\varepsilon = 10^{-5}$ . We illustrate the high accuracy of analytic kernel interpolation and the associated artifacts in two

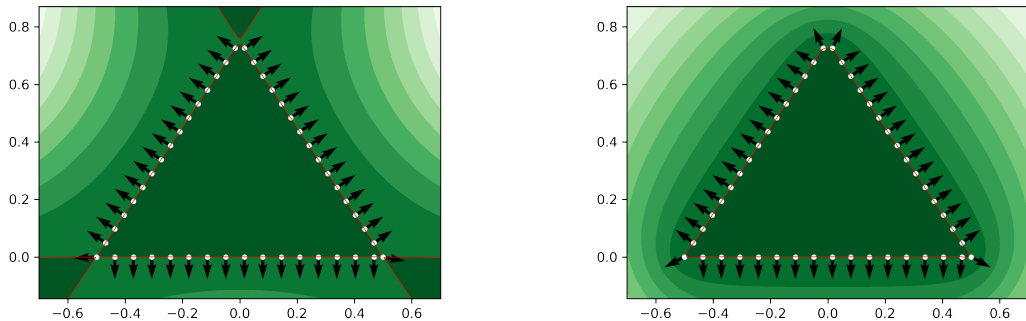


FIGURE 2. Reconstruction of a triangle from 48 sample points using Gauss and Laplace kernel interpolation, left and right, respectively.

examples of curves. In the first, see Figure 3, we compute the implied level set of the signature function of a sample consisting of points situated on one half of an ellipse, in the second (Figure 4) that of a full square and the same square with a missing corner. The first shows the ability of the method to perform analytic continuation. The second shows how the level sets of an analytic function attempt to accommodate the sample of a non-smooth curve. These latter examples underscore how the

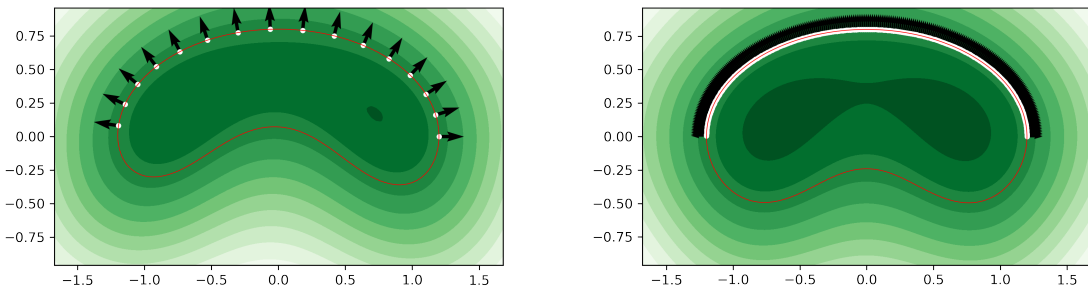


FIGURE 3. Implied curve of an exact sample consisting of  $m$  points along half of a ellipse. Left:  $m = 16$ . Right:  $m = 256$ .

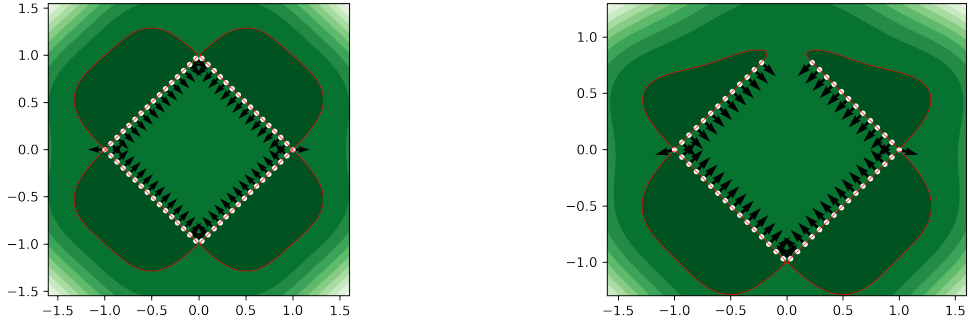


FIGURE 4. Implied curve of an exact sample of points of a full square and one with a corner removed.

disconnection problems reported in the literature and observed when using radial basis functions to interpolate scattered data is in good part due to the regularity of the chosen kernel (and the implied regularity of the interpolant) and not, as sometimes argued [4], to the local nature (read fast decay) of the kernel. In fact the problem can be all but resolved by using less regular kernels or by regularizing in the way described before.

**5.2. Quadratic Surfaces.** We briefly consider the case of quadratic surfaces (locally) in order to revisit the remark about “flat” points and to show that the method is capable of recovering an approximation to the actual principal curvatures if the symmetry is broken. We consider the surface defined by  $z = \frac{a}{2}x^2 - \frac{b}{2}y^2$  ( $a, b > 0$ ) and concentrate on the origin. When  $a \neq b$ , the method recovers an approximation to the principal curvatures. Indeed, taking the patch of the surface above  $[-.5, .5] \times [-.5, .5]$  and using a regular discretization of  $16 \times 16$  points, Gauss and regularized ( $\varepsilon = 1$ ) Laplace yield the results of Table 1. The same computation with  $a = b = 1$  gives the results of

Kernel	$\kappa_1$	$\kappa_2$
Gauss	$1.000 \times 10^0$	$-2.000 \times 10^0$
Laplace	$1.003 \times 10^0$	$-1.992 \times 10^0$

TABLE 1. Quadratic surface. Principal curvatures in the origin computed using Gauss and Laplace kernels for  $a = 1$  and  $b = 2$  using 256 points.

Table 2. In this case, the symmetry leads to very small gradients, their lengths are  $3.1948 \times 10^{-11}$  (Gauss) and  $5.6192 \times 10^{-12}$  (Laplace) and, hence, to a very inaccurate numerical estimation of the curvature. Interestingly, if one replaces the “regular” sample with a random sample of the domain

Kernel	$\kappa_1$	$\kappa_2$
Gauss	$-4.4615 \times 10^{10}$	$-3.1650e \times 10^5$
Laplace	$-3.8913 \times 10^9$	$3.5405 \times 10^7$

TABLE 2. Quadratic surface. Principal curvatures in the origin computed using Gauss and Laplace kernels for  $a = b = 1$  using 256 points.

(uniform distribution), Laplace interpolation (less ill-posed) is able to recover the actual curvatures. Indeed for a random sample of the same size, one obtains

$$\kappa_1 = 9.8534 \times 10^{-1}, \kappa_2 = -1.0138 \times 10^0,$$

an approximation, which is consistent over many runs. As previously mentioned this is a problem encountered when only local information is available and disappears when dealing with closed smooth surfaces with a well-defined inside and outside.

**5.3. Laplace-Beltrami Operator of the Sphere.** We consider now the numerical computation of the Laplace-Beltrami operator of a function  $f$  given through its values  $\mathbb{Y}$  at the  $m$  points  $\mathbb{X}$  of the Fibonacci discretization of the unit sphere<sup>†</sup>. In Table 3, we report the average relative  $L^\infty$ -error at 32 randomly chosen points on the sphere (and hence unrelated to the discretization points) in the values of the function, its surface gradient, and Laplace-Beltrami operator applied to it. The function chosen

$m$	$f$ error	$\nabla_{\mathbb{S}^2} f$ error	$\Delta_{\mathbb{S}^2} f$ error
64	$3.811 \times 10^{-2}$	$3.857 \times 10^{-1}$	$5.673 \times 10^{-1}$
128	$8.538 \times 10^{-4}$	$1.579 \times 10^{-1}$	$1.654 \times 10^{-2}$
256	$2.623 \times 10^{-6}$	$4.271 \times 10^{-5}$	$3.136 \times 10^{-5}$
512	$1.117 \times 10^{-9}$	$2.971 \times 10^{-8}$	$1.268 \times 10^{-8}$

TABLE 3. Average relative  $L^\infty$ -error at different discretization levels  $m$  for function evaluation (interpolation), surface nabla, and Laplace-Beltrami evaluation.

is  $f(x) = \sin(\pi(1 + 2x_3))$  and we work with the Laplace kernel with  $\varepsilon = 1$ . The exact surface nabla and Laplace-Beltrami can be computed

$$\begin{aligned} \nabla_{\mathbb{S}^2} f(x) &= 2\pi \cos(\pi(1 + 2x_3)) \begin{bmatrix} -x_1 x_2 & -x_2 x_3 & 1 - x_3 \end{bmatrix}^\top \\ \Delta_{\mathbb{S}^2} f(x) &= 8\pi(x_3^2 - 1) \sin(\pi(1 + 2x_3)) - 4\pi x_3 \cos(\pi(1 + 2x_3)) \end{aligned}$$

for  $x \in \mathbb{S}^2$  and compared to the numerical values obtained with the method developed in Section 3.2 using  $u_{\mathbb{X}}$ ,  $\nu_{\mathbb{X}}$ ,  $H_{\mathbb{X}}$ , and  $u_{\mathbb{X},\mathbb{Y}}$ . We underline the fact that the method has only knowledge of  $f$  at a sample of points on the sphere and that  $u_{\mathbb{X},\mathbb{Y}}$  is an extension of  $f|_{\mathbb{X}}$  that, yes, interpolates  $f$  on  $\mathbb{S}^2$  but can be quite different away from the sphere. In particular its gradient and Hessian can have “little” to do with those of  $f$ .

**5.4. The Ring Torus.** In this section we illustrate how the method computes the principal curvatures of a torus parametrized by

$$([R_1 + R_2 \cos(v)] \cos(u), [R_1 + R_2 \cos(v)] \sin(u), R_2 \sin(u)), \quad u, v \in [0, 2\pi),$$

where  $R_1 = 2$  and  $R_2 = .5$ . The curvatures are given by  $\kappa_1 = -2$  and  $\kappa_2 = \frac{\cos(v)}{R_1 + R_2 \cos(v)}$ , i.e. one is the curvature of any of the vertical circles, while the other depends on the height of the point considered as well as its distance to the origin. For this reason we choose  $u \in [0, 2\pi)$  at random, fix it, and compute the curvatures numerically at 32 equidistant points on the corresponding vertical circle. The signature function  $u_{\mathbb{X}}$  is computed for samples of size  $|\mathbb{X}| = 64, 128, 256, 512, 1024$ . These samples are obtained in two different ways. The first consists in picking  $u, v$  independently and uniformly at random from  $[0, 2\pi)$  and then accepting the sample  $(u, v)$  with a probability corresponding to the normalized surface

<sup>†</sup>The basic idea is to use the golden ratio to generate a non-closing spiral of points on the sphere to obtain an almost uniform distribution (see [30, 16]).

area at the corresponding point (see [12]). The second is based on the Fibonacci lattice, which, while deterministic, does avoid clustering and is almost uniform. For the first sampling method, Table 4 shows the  $L^\infty$  and  $L^2$  relative errors in the two curvatures (ordered by size), while the samples are depicted in Figure 5. In all experiments we use  $\alpha = 10^{-10}$  for both kernels (thus introducing a limit to the achievable accuracy) and  $\varepsilon = 1$  for the Laplace kernel.

$m$	$L^\infty$ (Gauss)	$L^2$ (Gauss)	$L^\infty$ (Laplace)	$L^2$ (Laplace)
64	$1.85 \times 10^{-1} / 1.72 \times 10^{-1}$	$9.88 \times 10^{-2} / 4.41 \times 10^{-2}$	$1.02 \times 10^{-1} / 2.21 \times 10^{-1}$	$2.20 \times 10^{-1} / 1.33 \times 10^{-1}$
128	$1.77 \times 10^{-2} / 1.61 \times 10^{-2}$	$1.41 \times 10^{-2} / 5.24 \times 10^{-3}$	$5.26 \times 10^{-2} / 1.08 \times 10^{-1}$	$1.72 \times 10^{-2} / 9.56 \times 10^{-3}$
256	$5.09 \times 10^{-5} / 1.74 \times 10^{-4}$	$8.33 \times 10^{-4} / 2.75 \times 10^{-4}$	$8.61 \times 10^{-3} / 7.94 \times 10^{-3}$	$2.01 \times 10^{-3} / 9.18 \times 10^{-4}$
512	$2.23 \times 10^{-8} / 1.19 \times 10^{-7}$	$2.25 \times 10^{-7} / 7.86 \times 10^{-8}$	$1.59 \times 10^{-3} / 9.46 \times 10^{-4}$	$1.08 \times 10^{-3} / 3.64 \times 10^{-4}$
1024	$1.75 \times 10^{-8} / 1.36 \times 10^{-8}$	$5.99 \times 10^{-8} / 2.33 \times 10^{-8}$	$8.51 \times 10^{-6} / 4.18 \times 10^{-6}$	$3.78 \times 10^{-6} / 1.39 \times 10^{-6}$

TABLE 4. Randomly sampled torus. Relative  $L^\infty$  and  $L^2$  errors for Gauss and Laplace kernels at different values of  $m$ . Each entry shows the error values for the two principal curvatures ordered according to size.

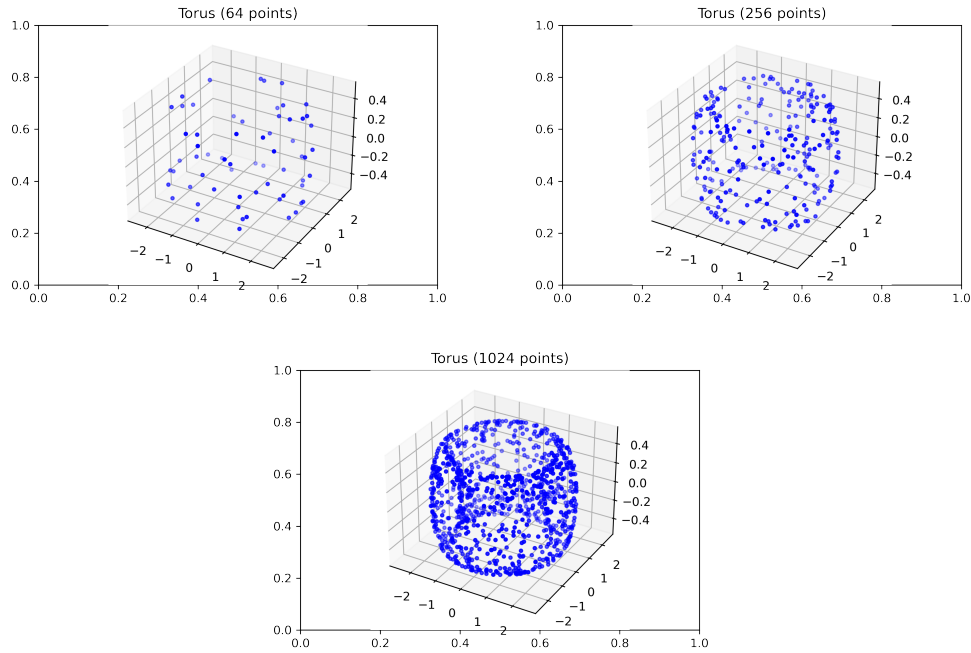


FIGURE 5. The samples obtained with a probability distribution proportional to the surface area.

Table 5 and Figure 6 show the corresponding results obtained using the Fibonacci lattice method.

$m$	$L^\infty$ (Gauss)	$L^2$ (Gauss)	$L^\infty$ (Laplace)	$L^2$ (Laplace)
64	$2.75 \times 10^{-1} / 2.39 \times 10^{-1}$	$1.86 \times 10^{-1} / 9.61 \times 10^{-2}$	$1.24 \times 10^{-1} / 1.08 \times 10^{-1}$	$8.90 \times 10^{-2} / 5.06 \times 10^{-2}$
128	$1.01 \times 10^{-2} / 9.62 \times 10^{-3}$	$1.48 \times 10^{-2} / 6.71 \times 10^{-3}$	$4.42 \times 10^{-2} / 3.27 \times 10^{-2}$	$2.53 \times 10^{-2} / 1.18 \times 10^{-2}$
256	$3.39 \times 10^{-4} / 2.36 \times 10^{-4}$	$1.66 \times 10^{-4} / 6.53 \times 10^{-5}$	$3.00 \times 10^{-3} / 2.08 \times 10^{-3}$	$5.84 \times 10^{-4} / 2.64 \times 10^{-4}$
512	$3.35 \times 10^{-7} / 2.31 \times 10^{-7}$	$2.64 \times 10^{-7} / 8.60 \times 10^{-8}$	$3.11 \times 10^{-4} / 2.08 \times 10^{-4}$	$3.34 \times 10^{-5} / 1.64 \times 10^{-5}$
1024	$9.93 \times 10^{-10} / 8.59 \times 10^{-10}$	$1.28 \times 10^{-8} / 6.10 \times 10^{-9}$	$1.16 \times 10^{-6} / 7.40 \times 10^{-7}$	$4.79 \times 10^{-7} / 1.85 \times 10^{-7}$

TABLE 5. Fibonacci lattice on the torus. Relative  $L^\infty$  and  $L^2$  errors for Gauss and Laplace kernels at different values of  $m$ . Each entry shows the error values for the two principal curvatures ordered according to size.

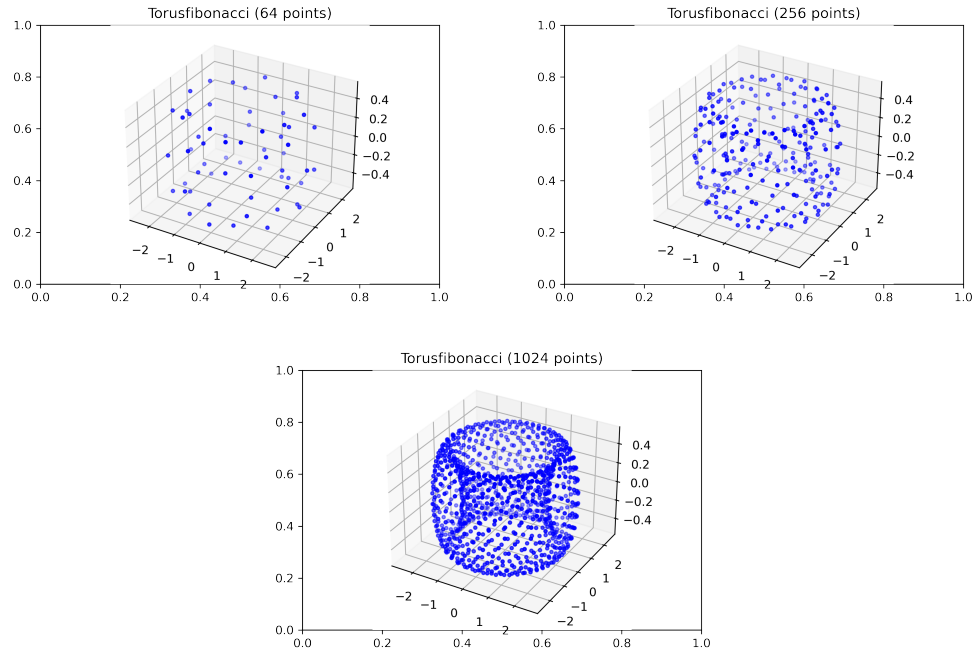


FIGURE 6. The Fibonacci samples used.

**5.5. The Gauss Curvature of an Ellipsoid.** Consider the ellipsoid  $[\frac{x_1^2}{a^2} + \frac{x_2^2}{b^2} + \frac{x_3^2}{c^2} = 1]$  with  $a = 2$ ,  $b = .5$ ,  $c = 1$  and a Fibonacci discretization  $\mathcal{X}$  consisting of  $m$  points. Use the latter to approximate its Gauss curvature

$$K = \kappa_1 \kappa_2 = \frac{1}{a^2 b^2 c^2 \left( \frac{x_1^2}{a^4} + \frac{x_2^2}{b^4} + \frac{x_3^2}{c^4} \right)^2}$$

at 32 randomly chosen points (we first choose points uniformly on the sphere using a normal distribution in the ambient space and normalize, then scale their components by  $a$ ,  $b$ , and  $c$ , respectively). Table 6 record the relative error observed when using the Laplace kernel with  $\varepsilon = 1$  and different discretization levels.

**5.6. The Noisy Case.** The framework developed allows one to seemlessly replace interpolation with approximate interpolation by simply replacing the hard constraint by a fidelity term. It is interesting that, in this context, this regularization is also reflected in the level sets of the signature function and

$ \mathbb{X} $	64	128	256	512	1024
Relative error	$2.428 \times 10^{-1}$	$8.408 \times 10^{-2}$	$1.186 \times 10^{-2}$	$5.439 \times 10^{-4}$	$4.995 \times 10^{-5}$

TABLE 6. Gauss curvature error for an ellipsoid.

hence has a geometric effect on the level sets. We illustrate this with a few numerical experiments. We consider curves again here since they are easier to visualize. In Figure 7 we depict the reconstruction (in red) of an ellipse based on an equispaced (in parameter domain) sample of 32 points which are moved in a uniformly chosen random direction by a uniformly random distance in  $[0, 0.1]$  and give rise to  $\mathbb{X}$ . The red curve corresponds to the level  $\bar{u}_{\mathbb{X}}$  given by

$$\bar{u}_{\mathbb{X}} = \frac{1}{|\mathbb{X}|} \sum_{x \in \mathbb{X}} u_{\mathbb{X}}(x),$$

i.e. the average value of the signature function on the data set (which would be 1 for exact interpolation). Notice that we used the regularization parameter  $\alpha = .1$  to counteract the effect of noise. We also visualize the implied normals as well as the implied sublevel sets as explained at the beginning of the section. In addition we also draw in yellow the implied level 1 of the exact interpolant computed on the unperturbed data set (no noise) to provide an idea of the quality of the reconstruction. Notice

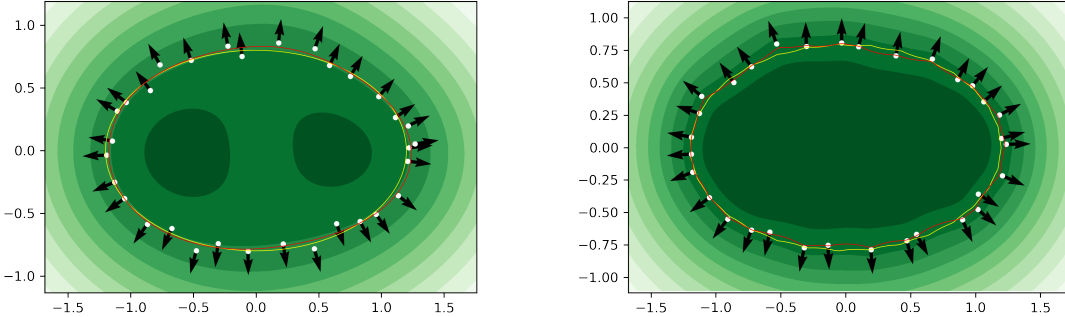


FIGURE 7. Reconstruction of an ellipse from a randomly perturbed sample of its points. The Gauss kernel is used on the left, while on the right the Laplace kernel is used with  $\varepsilon = 10^{-5}$ .

how the Laplace kernel (with little regularization  $\varepsilon = 10^{-5}$ ) exhibits high curvature at points in  $\mathbb{X}$  and in the original data set (not directly shown). If the Laplace kernel is regularized more ( $\varepsilon = 1$ ), then it performs similarly to the Gauss kernel as depicted in Figure 8 (left). The right picture in Figure 8 shows the reconstruction obtained with the Laplace kernel ( $\varepsilon = 1$ ) when each orginal datum is independently moved in a uniformly distributed random direction to a random distance uniformly chosen in  $[0, 0.25]$ .

**Remark 5.2.** *Finally we remark that, in some circumstances, it may be advantageous to use different kernels; one to obtain geometric information about  $\mathbb{X}$  and one to interpolate the values  $\mathbb{Y}$ . This could be the case when dealing with functions of limited regularity defined on a smooth manifold.*

## REFERENCES

[1] Nachman Aronszajn and Kenneth T. Smith. Theory of Bessel potentials. part i. *Annales de l'Institut Fourier*, 11(1):385–475, 1961.

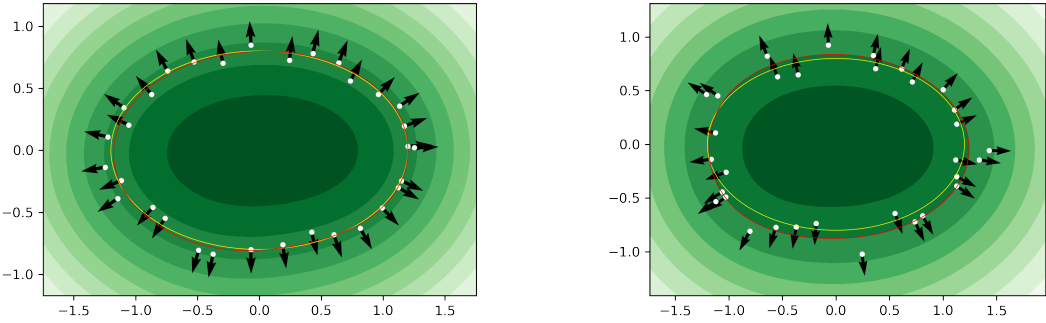


FIGURE 8. Reconstruction of an ellipse from a randomly perturbed sample of its points. The Laplace kernel is used with  $\varepsilon = 1$ .

- [2] Matthew Berger, Andrea Tagliasacchi, Lee M. Seversky, Pierre Alliez, Gaël Guennebaud, Joshua A. Levine, Andrei Sharf, and Claudio T. Silva. A survey of surface reconstruction from point clouds. *Computer Graphics Forum*, 36(1):301–329, 2017.
- [3] S. Brenner and L. Scott. *The Mathematical Theory of Finite Element Methods*. Springer, New York, 1994.
- [4] Jonathan C. Carr, Richard K. Beatson, Jon B. Cherrie, Tim J. Mitchell, Warren R. Fright, Bruce C. McCallum, and Toby R. Evans. Reconstruction and representation of 3d objects with radial basis functions. In *Proceedings of the 28th Annual Conference on Computer Graphics and Interactive Techniques (SIGGRAPH '01)*, pages 67–76. ACM, 2001.
- [5] Jonathan C. Carr, Richard K. Beatson, Bruce C. McCallum, W. Richard Fright, Trevor J. McLennan, and Tim J. Mitchell. Smooth surface reconstruction from noisy range data. In *Proceedings of the 1st International Conference on Computer Graphics and Interactive Techniques in Australasia and South East Asia, GRAPHITE '03*, pages 119–126, New York, NY, USA, 2003. ACM.
- [6] Ulrich Clarenz, Udo Diewald, and Martin Rumpf. A multiscale fairing method for textured surfaces. In Hans-Christian Hege and Konrad Polthier, editors, *Visualization and Mathematics III*, pages 245–260. Springer-Verlag, Heidelberg, 2003.
- [7] Naci Demirci and Megan A. Holland. Cortical thickness variation with curvature: A population study. *Brain Structure and Function*, 2022.
- [8] Mathieu Desbrun, Mark Meyer, Peter Schröder, and Alan H. Barr. Implicit fairing of irregular meshes using diffusion and curvature flow. In *Proceedings of the 26th Annual Conference on Computer Graphics and Interactive Techniques (SIGGRAPH '99)*, pages 317–324. ACM Press/Addison-Wesley Publishing Co., 1999.
- [9] Charlie Duclut, Aboutaleb Amiri, Joris Pajjmans, and Frank Jülicher. Coarse-grained curvature tensor on polygonal surfaces. *SciPost Phys. Core*, 5(1):011, 2022. Published 11 March 2022.
- [10] Gregory E. Fasshauer and Michael J. McCourt. *Kernel-Based Approximation Methods Using MATLAB*, volume 19 of *Interdisciplinary Mathematical Sciences*. World Scientific Publishing Co., Singapore, 2015.
- [11] Bruce Fischl and Anders M. Dale. Measuring the thickness of the human cerebral cortex from magnetic resonance images. *PNAS*, 2000.
- [12] James D. Foley, Andries van Dam, Steven K. Feiner, and John F. Hughes. *Computer Graphics: Principles and Practice*. Addison-Wesley Professional, Boston, 2nd edition, 1996.
- [13] Edward J. Fuselier and Grady B. Wright. Scattered data interpolation on embedded submanifolds with restricted positive definite kernels: Sobolev error estimates. *SIAM Journal on Numerical Analysis*, 50(3):1753–1776, 2012.
- [14] Michael Garland and Paul S. Heckbert. Surface simplification using quadric error metrics. In *SIGGRAPH '97 Conference Proceedings*, pages 209–216, August 1997.
- [15] Tim Gatzke and Cindy Grimm. Estimating curvature on triangular meshes. *International Journal of Shape Modeling*, 2006.
- [16] Alvaro González. Measurement of areas on a sphere using Fibonacci and latitude–longitude lattices. *Mathematical Geosciences*, 42(1):49–64, 2010.
- [17] P. Guidotti. Extracting manifold information from point clouds. *arXiv preprint*, 2025.
- [18] Paul S. Heckbert and Michael Garland. Optimal triangulation and quadric-based surface simplification. *Journal of Computational Geometry: Theory and Applications*, 14(1–3):49–65, November 1999.

- [19] Hugues Hoppe, Tony DeRose, Tom Duchamp, John McDonald, and Werner Stuetzle. Surface reconstruction from unorganized points. In *Proceedings of the 19th Annual Conference on Computer Graphics and Interactive Techniques, SIGGRAPH '92*, pages 71–78, New York, NY, USA, 1992. ACM.
- [20] Evangelos Kalogerakis, Patricio Simari, Derek Nowrouzezahrai, and Karan Singh. Robust statistical estimation of curvature on discretized surfaces. In *Proceedings of the Fifth Eurographics Symposium on Geometry Processing (SGP)*, pages 13–22. Eurographics Association, 2007.
- [21] Jan J. Koenderink and Andrea J. van Doorn. Surface shape and curvature scales. *Image and Vision Computing*, 10(8):557–564, 1992.
- [22] Bertil Matérn. *Spatial Variation*, volume 36 of *Lecture Notes in Statistics*. Springer-Verlag, Berlin, 2 edition, 1986.
- [23] Mark Meyer, Mathieu Desbrun, Peter Schröder, and Alan H. Barr. Discrete differential-geometry operators for triangulated 2-manifolds. In *Visualization and Mathematics III*, pages 35–57. Springer, 2003.
- [24] Henry P. Moreton and Carlo H. Séquin. Functional minimization for fair surface design. In *SIGGRAPH '92 Conference Proceedings*, pages 167–176, July 1992.
- [25] Bryan S. Morse, Terry S. Yoo, Penny Rheingans, David T. Chen, and K. R. Subramanian. Interpolating implicit surfaces from scattered surface data using compactly supported radial basis functions. In *Proceedings of the International Conference on Shape Modeling and Applications, SMI '01*, pages 89–98, Washington, DC, USA, 2001. IEEE.
- [26] Yutaka Ohtake, Alexander Belyaev, and Hans-Peter Seidel. A multi-scale approach to 3D scattered data interpolation with compactly supported basis functions. In *Proceedings of the Shape Modeling International 2003, SMI '03*, pages 153–161, Washington, DC, USA, 2003. IEEE Computer Society.
- [27] Cécile Piret. The orthogonal gradients method: a radial basis functions method for solving partial differential equations on arbitrary surfaces. *Journal of Computational Physics*, 231(14):4662–4675, 2012.
- [28] Carl E. Rasmussen and Christopher K. I. Williams. *Gaussian Processes for Machine Learning*. MIT Press, 2006.
- [29] S.-A. Sadegh-Zadeh et al. Curvature estimation and machine learning for neurodegenerative disease diagnosis: A systematic review. *NeuroImage: Clinical*, 2025.
- [30] R. Swinbank and R. J. Purser. Fibonacci grids: A novel approach to global modelling. *Quarterly Journal of the Royal Meteorological Society*, 132(619):1769–1793, 2006.
- [31] Gabriel Taubin. Estimating the tensor of curvature of a surface from a polyhedral approximation. In *Proceedings of ICCV*, pages 902–907, 1995.
- [32] Grace Wahba. *Spline Models for Observational Data*, volume 59 of *CBMS-NSF Regional Conference Series in Applied Mathematics*. Society for Industrial and Applied Mathematics, Philadelphia, PA, 1990.
- [33] M. Welk, D. Theis, T. Brox, and J. Weickert. PDE-Based Deconvolution with Forward-Backward Diffusivities and Diffusion Tensors. In R. Kimmel, N. Sochen, and J. Weickert, editors, *Scale Space 2005*, LNCS 3459, pages 585–597. Springer Verlag, 2005.
- [34] H. Wendland. *Scattered Data Approximations*. Number 17 in Cambridge Monographs on Applied and Computational Mathematics. Cambridge University Press, Cambridge, 2004.
- [35] Holger Wendland. Fast evaluation of radial basis functions: methods based on partition of unity. In *Approximation Theory X: Wavelets, Splines, and Applications*, pages 473–483. Vanderbilt University Press, Nashville, TN, 2002.

UNIVERSITY OF CALIFORNIA, IRVINE, DEPARTMENT OF MATHEMATICS, 340 ROWLAND HALL, IRVINE, CA 92697-3875, USA

Email address: [gpatrick@math.uci.edu](mailto:gpatrick@math.uci.edu)